Dual-Frequency Decoupling for Two Distinct Antennas

Mohammed M. Albannay, *Student Member, IEEE,* Jacob C. Coetzee, *Member, IEEE,* Xinyi Tang, *Member, IEEE* and Koen Mouthaan, *Member, IEEE*

***Abstract*—Constant development of new wireless standards increases the demand for more radiating elements in compact end-user platforms. A decrease in antenna separation gives rise to increased antenna coupling, resulting in a reduction of the signal-to-interference-plus-noise-ratio (SINR) between transmitter and receiver. This paper proposes a decoupling network which provides dual band port isolation for a pair of distinct antennas. A prototype has been fabricated to verify the theory.**

***Index Terms*—Dual-band decoupling, decoupling network, port isolation, mutual coupling.**

I. Introduction

DEMAND for high performance, reliability and data rate communication has catalyzed the evolution of wireless standards in the past three decades [1] . Consequently, modern end-user platforms are equipped with miniaturized antennas to operate with the latest standards whilst allowing for backward compatibility. It is common practice in the wireless industry to allocate a distinct radiator for each operating band cluster in the end-user platform. User equipment manufacturers are constantly decreasing the physical dimensions of the platform to enhance aesthetics and utility. This inevitably leads to aggravated mutual coupling between closely spaced radiators. Mutual coupling causes feedback looping between radiators [2], [3]. This in turn decreases SINR, which causes significant transmission degradation [3].

This intrinsic problem can be overcome with the use of miniaturized surface acoustic wave (SAW) duplexers [4], utilizing a frequency division duplex (FDD) scheme. This approach occupies a very small footprint, but its complex architecture makes it difficult to design and fabricate for arbitrary frequency bands. A miniaturized microstrip diplexer is discussed in [5]. It provides dual-band isolation, but tailoring the design for an arbitrary pair of frequencies would also require significant effort. Suspended neutralizing lines are used in [6] to reduce coupling between two planar inverted-F antennas. While the solution is simple in principle, it lacks a robust design procedure and is difficult to implement in practice.

An alternative approach to overcoming mutual coupling is through the use of a passive decoupling network to obtain port isolation. In its simplest form, a decoupling network consists of reactive components connected between neighboring antennas. Typically, a decoupling network for an N port antenna array is a $2N$ port network, incorporating reactive components and/or transmission line sections and/or stubs. Port isolation between two identical antennas has been achieved for single band [7]–[9] and dual band cases [10], [11].

In this paper, a decoupling network for two closely spaced, distinct antennas operating at two different frequencies is introduced. It provides a matched port for each of the frequencies while maintaining isolation at both frequencies. The theory is validated by measurements on a fabricated prototype.

II. Theory and Design of Decoupling Network

The distinct antenna pair in Fig. 1 is characterized by scattering matrix $\mathbf{S^a}$, given by

$$\mathbf{S^a} = \begin{bmatrix} S_{11}^a & S_{12}^a \\ S_{12}^a & S_{22}^a \end{bmatrix}, \tag{1}$$

where $S_{11}^a \neq S_{22}^a$. The corresponding admittance matrix can be calculated from

$$\mathbf{Y^a} = Y_0(\mathbf{I} - \mathbf{S^a})(\mathbf{I} + \mathbf{S^a})^{-1} = \begin{bmatrix} Y_{11}^a & Y_{12}^a \\ Y_{12}^a & Y_{22}^a \end{bmatrix}, \tag{2}$$

where $\mathbf{I}$ is an 2×2 identity matrix and Y_0 is the characteristic admittance of the system.

This pair of antennas can be decoupled using the circuit shown in Fig.1. It consists of two transmission lines with characteristic impedance Z_{01} and Z_{02} and electrical lengths θ_1 and θ_2. A shunt element with an admittance of jB completes the network. Using transmission line theory, the admittance matrix at ports $1'$ and $2'$ can be calculated from

$$\mathbf{Y'} = \mathbf{B}\,\mathbf{A}^{-1} = \begin{bmatrix} Y'_{11} & Y'_{12} \\ Y'_{12} & Y'_{22} \end{bmatrix}, \tag{3}$$

with

$$\mathbf{A} = \begin{bmatrix} \cos\theta_1 + jZ_{01}Y_{11}^a \sin\theta_1 & jZ_{01}Y_{12}^a \sin\theta_1 \\ jZ_{02}Y_{12}^a \sin\theta_2 & \cos\theta_2 + jZ_{02}Y_{22}^a \sin\theta_2 \end{bmatrix}$$

and

$$\mathbf{B} = \begin{bmatrix} Y_{11}^a \cos\theta_1 + j\sin(\theta_1)/Z_{01} & Y_{12}^a \cos\theta_1 \\ Y_{12}^a \cos\theta_2 & Y_{22}^a \cos\theta_2 + j\sin(\theta_2)/Z_{02} \end{bmatrix}.$$

M. M. Albannay and J. C. Coetzee are with the School of Electrical Engineering and Computer Science, Queensland University of Technology, Brisbane, QLD 4001, Australia (e-mail: albannay@student.qut.edu.au; jacob.coetzee@qut.edu.au).

X. Tang and K.Mouthaan are with the Department of Electrical and Computer Engineering, National University of Singapore, Singapore 119077, Singapore (e-mail: eletangx@nus.edu.sg; k.mouthaan@nus.edu.sg).

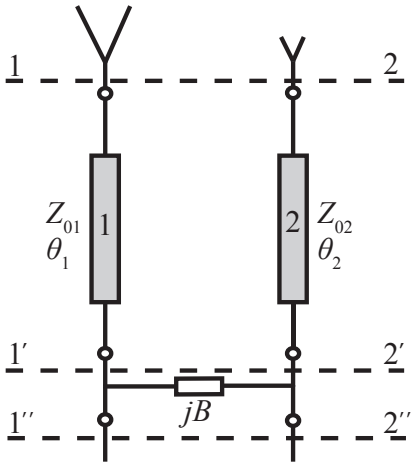

Fig. 1. Distinct antenna pair with decoupling network

With the addition of the parallel admittance jB, the admittance matrix at ports $1''$ and $2''$ becomes

$$\mathbf{Y}'' = \begin{bmatrix} G'_{11} + j(B'_{11} + B) & G'_{12} + j(B'_{12} - B) \\ G'_{12} + j(B'_{12} - B) & G'_{22} + j(B'_{22} + B) \end{bmatrix}. \quad (4)$$

For an arbitrary choice of Z_{01}, Z_{02} and θ_1, the electrical length θ_2 can be adjusted so that $G'_{12} = 0$. By selecting $B = B'_{12}$, equation (4) reduces to

$$\mathbf{Y}'' = \begin{bmatrix} G'_{11} + j(B'_{11} + B'_{12}) & 0 \\ 0 & G'_{22} + j(B'_{22} + B'_{12}) \end{bmatrix}. \quad (5)$$

The zero off-diagonal elements in (5) indicate that the ports are decoupled.

Port isolation for the antenna pair at two frequencies f_i $(i = 1, 2)$ is accomplished by calculating the characteristic impedances Z_{01} and Z_{02} as well as the required electrical lengths $\theta_1(f_i)$ and $\theta_2(f_i)$. The voltage reflection coefficient seen at ports $1''$ and $2''$ is given by

$$|\Gamma_i| = \left| \frac{Y_0 - Y''_{ii}}{Y_0 + Y''_{ii}} \right|. \quad (6)$$

An infinite number of solutions are available. The most appropriate solution is obtained by minimizing the mismatch at ports $1''$ and $2''$. A cost function $g = \max[|\Gamma_1(f_1)|, |\Gamma_2(f_2)|]$ can be used to optimize parameters Z_{01}, Z_{02}, $\theta_1(f_1)$ and $\theta_1(f_2)$, while $\theta_2(f_1)$ and $\theta_2(f_2)$ are computed during each iterative step of the optimization procedure by respectively solving

$$G'_{12}(f_i) = 0, \qquad i = 1, 2. \quad (7)$$

Subsequently, the susceptance of the shunt elements is obtained as $B(f_i) = B'_{12}(f_i)$.

III. Implementation of Decoupling Network

Transmission lines with specified values of electrical length at two different frequencies can be realized by composite left/right handed transmission lines [12]. However, this approach would require a large number of lumped elements. A simplified approach can be adopted by using a simple transmission line section with characteristic impedance Z_{01} and electrical length $\theta_1(f_1)$ for line 1 in Fig. 1. For this transmission line, the electrical length $\theta_1(f_2)$ has a predetermined value of

$$\theta_1(f_2) = \frac{f_2}{f_1}\,\theta_1(f_1). \quad (8)$$

The parameter $\theta_1(f_2)$ is thus no longer be available for the minimization of the cost function, leaving only Z_{01}, Z_{02} and $\theta_1(f_1)$ as variables for the optimization procedure. For line 2, a high-pass/band-pass filter cascade can be employed, as shown in Fig. 2. The topologies of the two filters are shown in Fig. 3. The required phase relation of the high-pass and band-pass filter is given by

$$\phi_{HPF}(f_i) + \phi_{BPF}(f_i) = -\theta_2(f_i), \qquad i = 1, 2. \quad (9)$$

The band-pass filter is designed at a center frequency of $f_0 = \sqrt{f_1 f_2}$ and produces an antisymmetric phase response at frequencies f_1 and f_2, so that

$$\phi_{BPF}(f_1) = -\phi_{BPF}(f_2). \quad (10)$$

From (9) and (10), it follows that

$$\phi_{HPF}(f_1) + \phi_{HPF}(f_2) = -\theta_2(f_1) - \theta_2(f_2), \quad (11)$$

with $\phi_{HPF}(f_i)$ defined as [13]

$$\phi_{HPF}(f_i) = \tan^{-1}\left(\frac{4\pi C f_i Z_{02}}{(2\pi C f_i Z_{02})^2 - 1} \right). \quad (12)$$

The capacitance C can be found by solving the non-linear equation (11). Subsequently, L can be calculated from [13]

$$L = \frac{Z_{02}}{2\pi f_1 \sin\left(\phi_{HPF}(f_1)\right)}. \quad (13)$$

From (9), the required phase shift of the band-pass filter is

$$\phi_{BPF}(f_1) = -\phi_{HPF}(f_1) - \theta_2(f_1). \quad (14)$$

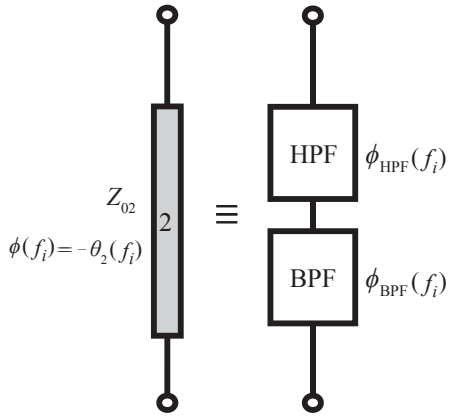

Fig. 2. Implementation of line 2 with a high-pass filter cascaded to a band-pass filter to simultaneously realize the required phase shift $\phi(f_1)$ and $\phi(f_2)$.

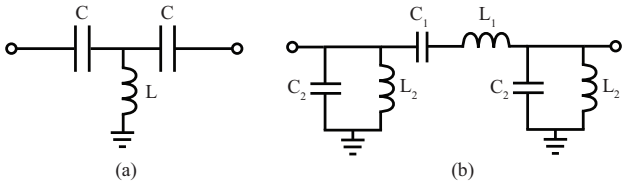

Fig. 3. Topology of (a) high-pass filter and (b) band-pass filter.

The component values for the band-pass filter are given by [13]

$$L_1 = rb\frac{Z_{02}}{2\pi f_0} \qquad L_2 = \frac{Z_{02}}{2\pi f_0 b}$$
$$C_1 = \frac{1}{2\pi r b f_0 Z_{02}} \qquad C_2 = \frac{b}{2\pi f_0 Z_{02}}, \tag{15}$$

where

$$r = \frac{1+\tan|\phi_{BPF}|^2+\sqrt{1+\tan|\phi_{BPF}|^2}}{1+\tan|\phi_{BPF}|^2} \tag{16}$$

and

$$b = \frac{f_r\sqrt{-1+2/r}}{1-f_r^2}, \tag{17}$$

with $f_r = f_1/f_0$ being the normalized frequency. The shunt susceptance $B(f_1)$ and $B(f_2)$ can be realized as a parallel or series LC circuit. Element values can be calculated using relations provided in [10].

Alternatively, a transmission line section can be used instead of the high-pass filter. The physical length of the transmission line with characteristic impedance of Z_{02} can be calculated by

$$l_{TL} = \frac{\theta_2(f_1)+\theta_2(f_2)}{2\pi(f_1+f_2)}v_p, \tag{18}$$

where v_p is the phase velocity of the line. From (9), the required phase shift from the band-pass filter would be

$$\phi_{BPF}(f_1) = \frac{2\pi f_1 l_{TL}}{v_p} - \theta_2(f_1). \tag{19}$$

IV. Measurement Results

To verify the theory, a pair of printed monopole antennas were used. The length of the monopoles were chosen to achieve resonance at $f_1 = 1.8$ GHz and $f_2 = 2.45$ GHz. Using the procedure described in Sections II and III, the design parameters were computed and are shown in Table I.

Discrete inductors and capacitors from Murata's LQW series and GJM series were used on Rogers RO4003 substrate ($\epsilon_r = 3.55$, $\tan\delta = 0.0027$, thickness = 0.81 mm) to realize the prototype. An Agilent Technologies 8510C Network Analyzer was used to measure the scattering parameters. The final prototype is displayed in Fig. 4. The antenna pair is characterized by the measured scattering parameters shown in Fig. 5. Port coupling $|S_{21}|$ is high, being -4.33 dB at f_1 and -6.25 dB at f_2. Note that the resonance of the two antennas is shifted from the original design values due to the effects of mutual coupling. Conventional stub matching networks were used to match the decoupled ports ($1''$ and $2''$) to the system impedance of $Z_0 = 50\ \Omega$, as seen in Fig. 4. However this is achieved at the penalty of reduced bandwidth, which is a common trait for decoupling circuits, as pointed out in [7] and [14]. This results in matched ports with increased isolation between them, as displayed in Fig. 6. The performance of the decoupling and matching network is summarized in Table II. Note that the quoted values for efficiency are simulated values which exclude metalization losses. The lower dissipation of the decoupling and matching network at the higher frequency is due to differences in current distribution at the two frequencies.

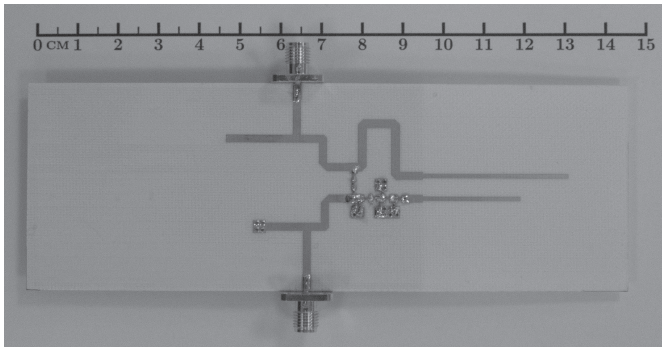

Fig. 4. Dual band monopole antenna pair with 4.5 mm separation with proposed decoupling network and single stub matching networks.

The option of using a transmission line section and band-pass filter to implement line 2 was also considered. Results showed that the transmission line and band-pass filter approach yields inferior bandwidth compared to the high-pass filter solution.

TABLE I
Design Parameters for Decoupling Network

Line 1 (Transmission Line)	Z_{01}	45 Ω
	$\theta_1(f_1)$	125°
	$\theta_1(f_2)$	170°
	Length	34.5 mm
	Track width	2.11 mm
Line 2 (Filters)	Z_{02}	46 Ω
	$\theta_2(f_1)$	320° (−40°)
	$\theta_2(f_2)$	344° (−16°)
High-pass filter	$\phi_{HPF}(f_1)$	32°
	$\phi_{HPF}(f_2)$	24°
	C	6.68 pF
	L	7.2 nH
Band-pass filter	$\lvert\phi_{BPF}(f_i)\rvert$	8°
	L_1	1.64 nH
	C_1	3.5 pF
	L_2	14.2 nH
	C_2	0.4 pF
Shunt Elements (Series LC circuit)	L	23.4 nH
	C	0.25 pF

TABLE II
Performance of Decoupling and Matching Network

Without decoupling & matching networks	Return Loss $\lvert S_{11}(f_1)\rvert$	−12.8 dB
	Return Loss $\lvert S_{22}(f_2)\rvert$	−13.1 dB
	Port Coupling $\lvert S_{21}(f_1)\rvert$	−4.33 dB
	Port Coupling $\lvert S_{21}(f_2)\rvert$	−6.25 dB
	Antenna Efficiency (f_1)	57.3%
	Antenna Efficiency (f_2)	71.2%
With decoupling & matching networks	Return Loss $\lvert S_{11}(f_1)\rvert$	−18.6 dB
	Return Loss $\lvert S_{22}(f_2)\rvert$	−22.4 dB
	Port Coupling $\lvert S_{21}(f_1)\rvert$	−22.6 dB
	Port Coupling $\lvert S_{21}(f_2)\rvert$	−28.2 dB
	Antenna Efficiency (f_1)	88.4%
	Antenna Efficiency (f_2)	85.2%

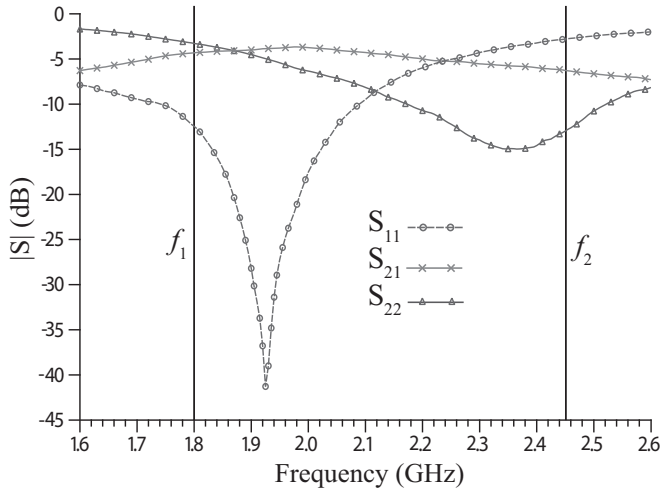

Fig. 5. Measured scattering parameters for the original antenna pair.

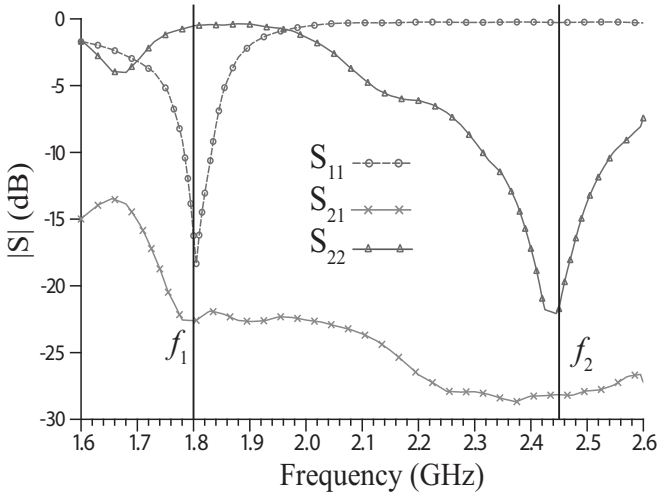

Fig. 6. Measured scattering parameters of antenna pair with decoupling and matching network.

V. Conclusion

This paper describes a method for achieving port isolation between two closely-spaced antennas operating at two different frequencies. The theory is verified by measured results on a fabricated prototype. The operating bandwidth with the addition of the decoupling and matching network can be improved by decreasing the initial mutual coupling and impedance mismatch observed at the antenna terminals. Note that the intention is to use a separate port for each of the frequencies while maintaining isolation at both frequencies. Isolated ports were therefore individually matched to only frequencies f_1 and f_2, respectively. Theoretically, the proposed design can be applied to an arbitrary set of frequencies. However, increased frequency separation may require higher order filter networks.

References

[1] T. Rappaport, A. Annamalai, R. Buehrer and W. Tranter, "Wireless communications: past events and a future perspective," *IEEE Commun. Mag.*, vol. 40, no. 5, pp. 148–161, May 2002.

[2] H.-S. Lui, H. T. Hui and M. S. Leong, "A note on the mutual-coupling problems in transmitting and receiving antenna arrays," *IEEE Antennas Propagat. Mag.*, vol. 51, pp. 171–176, Oct. 2009.

[3] J. Shi, Q. Luo and H. Sun, "Channel reciprocity of compact antenna array and the calibration," in *2011 IEEE 22nd Int. Symp. Personal Indoor* and *Mobile Radio Communication (PIMRC)*, Sept. 2011, pp. 1953–1957.

[4] H. Dong, T. Wu, K. Cheema, B. Abbott, C. Finch and H. Foo, "Design of miniaturized RF SAW duplexer package," *IEEE Trans. Ultrason. Ferroelectr. Freq. Control*, pp. 849–858, July 2004.

[5] T. Yang, P.-L. Chi and T. Itoh, "Compact quarter-wave resonator and its applications to miniaturized diplexer and triplexer," *IEEE Trans. Microw. Theory Tech.*, vol. 59, pp. 260–269, Feb. 2011.

[6] A. Diallo, C. Luxey, P. Le Thuc, R. Staraj and G. Kossiavas, "Study and reduction of the mutual coupling between two mobile phone PIFAs operating in the DCS1800 and UMTS bands," *IEEE Trans. Antennas Propag.*, vol. 54, pp. 3063–3074, Nov. 2006.

[7] J. Weber, C. Volmer, K. Blau, R. Stephan and M. Hein, "Miniaturized antenna arrays using decoupling networks with realistic elements," *IEEE Trans. Microw. Theory Tech.*, vol. 54, pp. 2733 –2740, June 2006.

[8] S.C. Chen, Y.S. Wang and S.J. Chung, "A decoupling technique for increasing the port isolation between two strongly coupled antennas," *IEEE Trans. Antennas Propag.*, vol. 56, pp. 3650–3658, Dec. 2008.

[9] J.C. Coetzee and Y. Yu, "Closed-form design equations for decoupling networks of small arrays," *Electron Lett.*, vol. 44, pp. 1441–1442, Dec. 2008.

[10] J. C. Coetzee, "Dual-frequency decoupling networks for compact antenna arrays," *Int. J. Microw. Sci. Technol.*, vol. 2011, pp. 3459–3466, 2011.

[11] X. Tang, K. Mouthaan and J. C. Coetzee, "Dual-band decoupling and matching network design for very closely spaced antennas," in *Proc. 2012 European Microwave Conference*, to be published.

[12] I.-H. Lin, M. DeVincentis, C. Caloz and T. Itoh, "Arbitrary dual-band components using composite right/left-handed transmission lines," *IEEE Trans. Microw. Theory Tech.*, vol. 52, pp. 1142–1149, April 2004.

[13] X. Tang and K. Mouthaan, "Design considerations for octave-band phase shifters using discrete components," *IEEE Trans. Microw. Theory Tech.*, vol. 58, pp. 3459–3466, Dec. 2010.

[14] H.J. Chalupka, X. Wang and J.C. Coetzee, "Compact arrays for mobile platforms: Trade-off between size and performance for SDMA and MIMO applications," in *Proc. 48th Internationales Wissenschaftliches Kolloquium*, Techniche Universität Ilmenau, 22–25 Sept. 2003.